Langmuir
Article
pubs.acs.org/Langmuir

Coffee-Ring Effect-Based Three Dimensional Patterning of Micro/Nanoparticle Assembly with a Single Droplet

Sun Choi,*[,†,‡] Stefano Stassi,[§,∥] Albert P. Pisano,[†,‡] and Tarek I. Zohdi[‡]

[†]*Berkeley Sensor and Actuator Center (BSAC), and* [‡]*Department of Mechanical Engineering, University of California at Berkeley, Berkeley, California 94720,* [§]*Center for Space Human Robotics, Corso Trento 21 Italian Institute of Technology at Polito, 10129 Torino, Italy, and* [∥]*Physics Department Politecnico di Torino, Corso Duca degli Abruzzi 24, 10129 Torino, Italy*

Received March 19, 2010. Revised Manuscript Received May 18, 2010

We develop a novel patterning technique to create 3D patterns of micro and nanoparticle assembly via evaporative self-assembly based on the coffee-ring effect of an evaporating suspension. The principle of the technique is analyzed theoretically by the scaling analysis of main parameters of the process and the scaling effect, the effect of the volume, the concentration of the suspension, and the effect of surface treatment on the patterning are studied. On the basis of the presented technique, we demonstrate that the patterns of 3D assembly of various sizes of microparticles (Silica), metal oxide nanoparticles (TiO_2, ZnO), and metallic nanoparticles (Ag) can be successfully generated by low-concentrated particle suspension (1.25−5 wt %) without additional sintering steps, and we also show the geometries of the patterns can be finely controlled by adjusting the parameters of the process.

Introduction

Creating regular, repetitive, and well-defined three-dimensional patterns of particle assembly in targeted area is a major bottleneck in various applications such as the fabrication of 3D photonic crystals,[1−3] printed electronics on flexible substrate,[4,5] colloidal quantum dot-based devices for display,[6−8] plasmonics,[9,10] and so forth. Previous approaches to pattern particle assembly, however, are required to use entire substrates without selective positioning of the assemblies,[11] chemically prepatterned substrates,[12−14] or soft-lithographic methods where applicable particles are largely constrained by molds and substrates.[15−17] There have been several attempts to control 2D micro and nanoparticle assembly from a liquid suspension.[16−28] In particular cases, the particles have been confined in various geometries of trenches by several approaches such as receding a contact line,[22−24] electrostatic force,[25] or assisted directed evaporation-induced self-assembly (ADEISA),[26−28] and the particles have been transported from the suspension to fill the trenches in as a result. In particular, it is reported that evaporation induced self-assembly of microparticles on modulated thickness show superb optical quality from which even intense optical refelectance spectra was measured.[26−28] These approaches require the fine control of the receding speed of contact line, the contact angle of meniscus of fluid with respect to the substrates[22−25] or an additional agitation of suspension with a long-channel, geometrical constraint.[26−28] Also, the release of the particle structure in the confined geometries, a crucial issue in the integration of the on-chip particle assembly with other microelectronic devices, has not yet been demonstrated. Moreover, most of the previous techniques are grounded on 2D interaction between the substrates and particle assembly; thus, structuring 3D particle assembly has been a huge challenge with those approaches. Evaporative self-assembly of meso, micro, and nanoscale particles[18−21] is well-known; interesting physical phenomenon at three-phase boundaries (particle−medium−air) and its applications[29−36] have been mainly restricted to fabricate planar structures because

*To whom correspondence should be addressed. Berkeley Sensor and Actuator Center (BSAC), University of California at Berkeley, Berkeley, California 94720, USA, Tel 510-643-9752, Fax 510-643-6637, E-mail: sunchoi@eecs.berkeley.edu.

(1) Joannopolous, J. D.; Villeneuve, P. R.; Fan, S. *Nature* **1997**, *386*, 143.
(2) Norris, D. J. *Nat. Mater.* **2007**, *6*, 177.
(3) Hynninen, A.; Thijssen, J. H. J.; Vermolen, E. C. M.; Dijkstra, M.; Blaaderen, A. V. *Nat. Mater.* **2007**, *6*, 202.
(4) Ahn, B. Y.; Duoss, E. B.; Motala, M. J.; Guo, X.; Park, S.; Xiong, Y.; Yoon, J.; Nuzzo, R. G.; Rogers, J. A.; Lewis, J. A. *Science* **2009**, *323*, 1590.
(5) Briseno, A. L.; Mannsfeld, S. C. B.; Ling, M. M.; Liu, S.; Tseng, R. J.; Reese, C.; Roberts, M. E.; Yang, Y.; Wudl, F.; Bao, Z. *Nature* **2006**, *444*, 913.
(6) Aoki, K.; Guimard, D.; Nishioka, M.; Nomura, M.; Iwamoto, S.; Arakawa, Y. *Nat. Photon.* **2008**, *2*, 688.
(7) Noda, S.; Fujita, M. *Nat. Photon.* **2009**, *3*, 129.
(8) Graham-rowe, D. *Nat. Photon.* **2009**, *3*, 307.
(9) Barnes, W. L.; Dereux, A.; Ebbesen, T. W. *Nature* **2003**, *424*, 824.
(10) Lal, S.; Link, S.; Halas, N. J *Nat. Photon.* **2007**, *1*, 641.
(11) Imhof, A.; Pine, D. J. *Nature* **1999**, *389*, 958.
(12) Qin, D.; Xia, Y.; Xu, B.; Yang, H.; Zhu, C.; Whitesides, G. M. *Adv. Mater.* **1999**, *11*, 1433.
(13) Lu, M. H.; Zhang, Y. *Adv. Mater.* **2006**, *18*, 3094.
(14) Fan, F.; Stebe, K. J. *Langmuir* **2004**, *20*, 3062.
(15) Park, I.; Ko, S. H.; Pan, H.; Grigoropoulos, C. P.; Pisano, A. P.; Fréchet, J. M. J.; Lee, E.; Jeong, J. *Adv. Mater.* **2008**, *20*, 489.
(16) Kim, E.; Xia, Y.; Whitesides, G. M. *Adv. Mater.* **1996**, *8*, 245.
(17) Kraus, T.; Malaquin, L.; Schmid, H.; Riess, W.; Spencer, N. D.; Wolf, H. *Nat. Nanotechnol.* **2007**, *2*, 570.
(18) Dushkin, C. D.; Yoshimura, H; Nagayama, K. *Chem. Phys. Lett.* **1993**, *204*, 455.
(19) Bowden, N.; Terfort, A.; Carbeck, J.; Whitesides, G. M. *Science* **1997**, *276*, 233.
(20) Denkov, N. D.; Velev, O. D.; Kralchevsky, P. A.; Ivanov, I. B.; Yoshimura, H.; Nagayama, K. *Nature* **1993**, *361*, 26.
(21) Rabani, E.; Reichman, D. R.; Geissler, P. L.; Brus, L. E. *Nature* **2003**, *426*, 271.
(22) Yin, Y; Lu, Y.; Gates, B.; Xia, Y. *J. Am. Chem. Soc.* **2001**, *123*, 8718.
(23) Su, G.; Guo, Q.; Palmer, R. E. *Langmuir* **2003**, *19*, 9669.
(24) Xiong, X.; Makaram, P.; Busnaina, A.; Bakhtari, K.; Somu, S.; McGrouer *Appl. Phys. Lett.* **2006**, *89*, 193108.
(25) Golding, R. K.; Lewis, P. C.; Kumacheva, E.; Allard, M.; Sargent, E. H. *Langmuir* **2004**, *20*, 1414.
(26) Yang, S. M.; Miquez, H.; Ozin, G. A. *Adv. Funct. Mater.* **2002**, *12*, 425.
(27) Miquez, H.; Yang, S. M.; Ozin, G. A. *Langmuir* **2003**, *19*, 3479.
(28) Miquez, H.; Yang, S. M.; Ozin, G. A. *Appl. Phys. Lett.* **2002**, *81*, 2493.
(29) Blaaderen, A. V. *Science* **1998**, *30*, 887.
(30) Fudouzi, H.; Xia, Y. *Langmuir* **2003**, *19*, 9653.
(31) Matsushita, S. I.; Yagi, Y.; Miwa, T.; Tryk, D. A.; Koda, T.; Fujishima, A. *Langmuir* **2003**, *16*, 636.
(32) Prevo, B. G.; Hon, E. W.; Velev, O. D. *J. Mater. Chem.* **2007**, *17*, 791.

technical difficulty lies in controlling interaction between the medium and the particles in 3D. In this paper, we demonstrate a unique and counterintuitive idea that the coffee-ring effect of an evaporating suspension can offer a governing method to create 3D patterns of micro/nanoparticle assembly via evaporative self-assembly. At first, the principle of the process is presented with qualitative descriptions. Provided the principle of the patterning, the patterns of 3D assembly of various sizes of microparticles (Silica), metal oxide nanoparticles (TiO_2, ZnO), and metallic nanoparticles (Ag) have been successfully fabricated by an evaporating, low-concentration particle suspension on the photopatterned substrate with proper surface treatment without any thermal or electrical sintering processes. Also, the geometries of the patterns were finely controlled by adjusting the parameters of the process. Then, the validity of the process is critically studied in-depth with the scaling analysis of main parameters of the process and the scaling effect, the effect of the volume, the concentration of the suspension, and the effect of surface treatment on the patterning are discussed as well.

Experimental Methods

Materials. A liquid suspension of silica microspheres (silicon dioxide-based microparticles; diameter, 0.5, 1, 3, and 5 μm; water, 95 wt %; silica 5 wt %; Sigma-Aldrich), Titanium oxide nanoparticles (diameter, 70 nm; water, 90 wt %; TiO_2, 10 wt %; Sigma-Aldrich), zinc oxide nanoparticles (diameter, 30 nm; water, 60 wt %; ZnO, 40 wt %; MK nano) have been diluted into various concentrations of suspension (2.5, 1.25, 0.625, and 0.3125 wt % silica) by adding a controlled volume of deionized water. A liquid suspension of silver nanoparticles (diameter, 7 nm; toluene, 70 wt %; Ag, 30 wt %) was synthesized according to the recipe in the literature.[37]

Design and Fabrication of Photopatterned Substrate. Various geometries of photomasks have been designed for the patterning. Various widths (4, 10, 20, 60, and 100 μm) and heights (2, 5, 10, 30, 50 μm) have been defined, and the combination of the width and the height of the trenches was chosen in such a way that the high-aspect ratio (=(height)/(width)) is constant at 0.5 while the lengths of the trenches vary according to the defined geometries. A lightly doped p-type silicon wafer (Silicon Quest International Inc.) was used as a substrate and SU-8 2005, 2010, 2030, 2050 (Microchem Corp.), SPR 220−7 (Megaposit), OIR 897−10I Positive I-line Photoresist (Fujifilm) was used as UV-sensitive photoresists. For the SU-8 patterns, SU-8 2005, 2010, 2030, and 2050 were spin-coated onto a silicon substrate at 3000 rpm for 30 s to achieve the thickness of 5, 10, 30, and 50 μm and soft-baked at 95 °C for 2, 3, 7, and 10 min, respectively. After UV-light exposure, the sample was baked at 95 °C for 2, 3, 6, and 10 min for postexposure bake and developed for 1, 2, 5, and 7 min. For the SPR 220−7 patterns, the photoresist was spin-coated onto a silicon substrate at 2200 rpm for 30 s (thickness ~10 μm) and soft-baked at 115 °C for 5 min. After UV-light exposure, the sample was developed for 4 min. For the I-line patterns, the photoresist was spin-coated on a silicon substrate at 2200 and 5000 rpm for 30 s to achieve the thickness of 2 and 1.2 μm, respectively, and soft-baked at 90 °C for 1 min. After the lithography step, oxygen plasma treatment (50 W, 260 mTorr, 30 s) enhanced the hydrophilicity of the patterned surface and the substrate.

Design of Experiments for Scaling Analysis. The scaling effect of the patterning is studied by the experiments of four different length scales. Silica microspheres whose diameters are 0.5, 1, 3, and 5 μm were used for the patterning of the dots whose widths are 10, 20, 60, and 100 μm, respectively. According to each particle size, four different concentrations (0.3125, 0.625, 1.25, and 2.5 wt %) of the suspension were used. The volume of the suspension used for the patterning was calculated in such a way that the number of particles per unit area of the patterning ((volume)/((patterning area) × (width)) is constant to 4×10^{-9} − 4.2×10^{-9} throughout the experiments of all the length scales. That results in the patterning of the same number of patterns. The volumes of 0.125, 1, 8, and 27 μL were used in the patterning of 0.5, 1, 3, and 5 μm of the silica microspheres, respectively.

Patterning of Micro/Nanoparticles. All the patterning experiments on the photopatterned substrate were conducted in air environment at atmospheric pressure and room-temperature conditions. Microsyringe (Microliter Syringes 5 μL, Hamilton) was used to extract a small volume (0.125−2.0 μL) of the micro/nanoparticle solution, and a single droplet was placed on the photopatterned substrate. After the particle assembly was completed, the sample was placed at room temperature for 1 h to evaporate the solvent completely and the photoresist was dissolved by either acetone or PRS 3000 Baker (J.T. Baker).

Imaging. The samples were imaged by optical microscope (Polylite 88, Reichert-Jung) and scanning electron microscopy (LEO 1550, *ZEISS*). A cross section of the channel was imaged after the sample was coated via the sputtering of a Au/Pd thin film.

Principle of 3D Patterning with a Single Droplet Based on Coffee-Ring Effect

Our technique is mainly grounded on the coffee-ring effect of solutes in an evaporating suspension. When a spilled drop of coffee dries on a solid surface, it leaves a dense, ring-like deposit along the perimeter. Such ring deposits are common wherever drops containing dispersed solids evaporate on a surface.[38] While a number of theoretical descriptions have been reported to estimate the growth rate of ring deposit,[38] velocity fields of a drying droplet,[39−41] and the dynamics of particle deposition,[42] applying the coffee-ring effect to pattern particle assembly has not been realized in current microfabrication technology. We demonstrate that photopatterns with proper surface treatment can be used as an effective template to structure particle assembly.

Preparation of Photopatterned Substrate. At first, conventional photoresist such as I-line (OIR 897−10I, Fujifilm) or SPR 220−7 (Megaposit) is spin-coated onto a substrate and patterned by UV exposure with followed development, and oxygen RF plasma is applied on the patterns. In case the medium of the particle suspension is hydrophilic as water is, a droplet of the suspension is placed on the pattern immediately after the surface treatment. Details on the preparation of photopatterned substrate are described in Experimental Methods. The oxygen plasma is used to make the surface hydrophilic and eliminate probable residue of the photoresist.

Descriptions of Sequential Processes of Self-Assembly of Particles. Figure 1 illustrates the sequential processes of the evaporative self-assembly of particles on photopatterned substrate. At first, a droplet of liquid suspension where micro or nanoparticles are well-dispersed is placed on the photopatterned

(33) Miyaki, M.; Fujimoto, K.; Kawaguchi, H. *Colloids Surf., A: Physiochem. Eng. Aspects* **1999**, *153*, 603.
(34) Kuncicky, D. M.; Prevo, B. G.; Velev, O. D. *J. Mater. Chem.* **2006**, *16*, 1207.
(35) Holland, B. R.; Blanford, C. F.; Do, T.; Stein *Chem. Mater.* **1999**, *11*, 795–805.
(36) Velev, O. D.; Tessier, P. M.; Lenhoff, A. M.; Kaler., E. W. *Nature* **1999**, *401*, 548.
(37) Wakuda, D.; Hatamura, M.; Suganuma, K. *Chem. Phys. Lett.* **2007**, *441*, 305.
(38) Deegan, R. D.; Bakajin, O.; Dupont, T. F.; Huber, G.; Nagel, S. R.; Witten, T. A. *Nature* **1997**, *389*, 827.
(39) Fischer, B. J. *Langmuir* **2002**, *18*, 60.
(40) Hu, H.; Larson, R. G. *Langmuir* **2005**, *21*, 3963.
(41) Hu, H.; Larson, R. G. *J. Phys. Chem. B* **2006**, *110*, 7090.
(42) Deegan, R. D. *Phys. Rev. E* **2000**, *61*, 475.

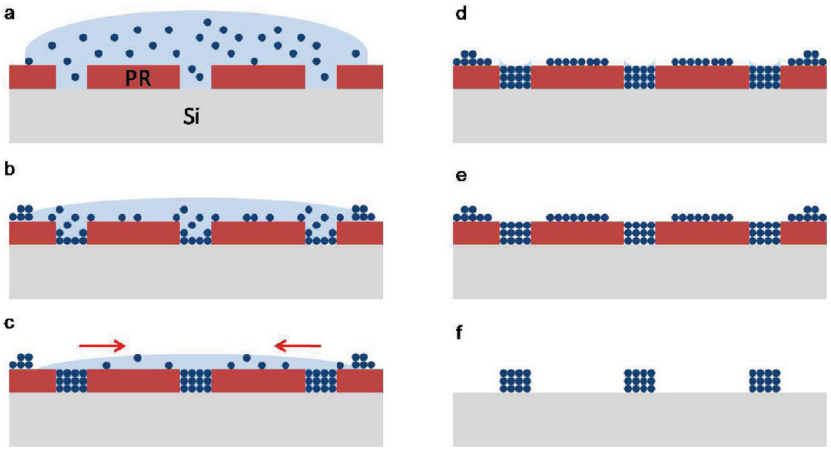

Figure 1. Schematics of the self-assembly of the microparticles on a photopatterned substrate. (a) A droplet of the suspension is placed on the patterned substrate. (b) The evaporation of the solvent is initiated. After contact-line pinning, the particle starts being confined. (c) After critical angle, the droplet starts receding. Confinement of the particles is completed. (d) Global evaporation is completed, the evaporation of local solvent forms tight assemblies of the particles. (e) The evaporation of the local fluid is completed. Tightly packed particle assemblies are formed. (f) The photoresist is removed. The patterns of particle assembly are formed.

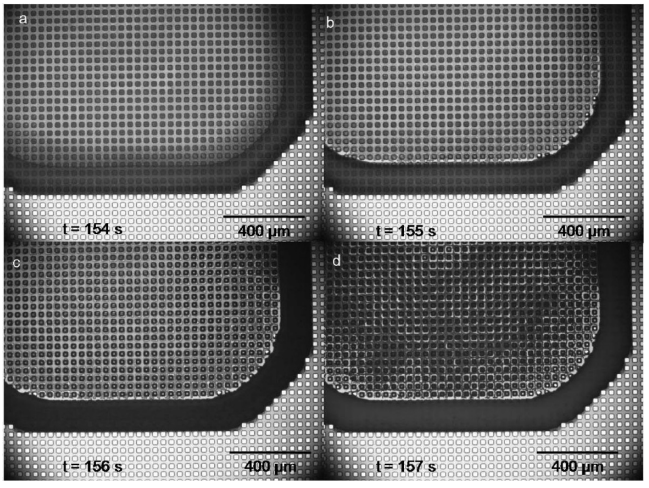

Figure 2. Snapshots of the particle assembly before the completion of the evaporation. (a) 3 s before the completion, the solutes are being transported to the peripheral region. (b) 2 s before the completion, depinning of the contact line is initiated. (c) 1 s before the completion, the evaporation of the local fluid is initiated. (d) The evaporation is completed. A thick, single coffee-ring deposit is generated at the edge of the droplet.

substrate. After that, the evaporation of the medium begins to occur and the particles are driven to the peripheral area of the droplet. This action of the particles, the coffee-ring effect, is mainly driven by the hydrodynamics of a drying droplet. It is reported[40] that the contact line of the droplet is pinned and the contact angle decreases for most of the drying time (98% of entire drying time). In this stage of the evaporation, the medium should flow from the center to the peripheral area to compensate for the loss of water; thus, the particles are also driven from the center to the peripheral region, creating a coffee-ring deposit. When the contact angle reaches the critical contact angle around 2−4°, the contact line starts receding and the evaporation of the droplet is completed.[40] The snapshots of the evaporating droplet are taken prior to the completion of the evaporation as shown in Figure 2. These snapshots show that the time consumed in depinning of the evaporating droplet is 3 s, which is only 1.9% of the overall drying time. A single, thick, coffee-ring deposit at the edge of the droplet is observed from the snapshots. It may be seemingly contradictory to the observation of multiple concentric rings after the evaporation of a single droplet in Adachi's work.[43] In Adachi's work, the volume fraction of the suspension is around 0.4−0.8%, which is much lower than the ones in our work, and the particle size was around 100 nm and a monolayer of the particles is deposited at the edge of the droplet. With the suspension of low-concentration suspension, the contact angle of the droplet is constantly maintained, and depinning and deposition of coffee-ring deposit are periodically repeated to form multiple concentric rings of the deposit. However, if the fraction of the suspension reaches around 0.3−2.5 wt % with larger particles as used in our work, the coffee-ring deposits consist of multiple layers of particle assembly and prevents depining of the contact line of an evaporating droplet. In our experimental platform, the overpressure gradient generated by the curvatures of the patterns[44] also locally drives the particles to the trenches formed by the patterns, while the particles are transported to the edge of the droplet globally. As can be seen from Figure 3, the particles inside the trenches and the particles on the photoresist are clearly separated throughout the entire droplet so that the lift-off process will not perturb the particle assembly inside the trenches. The separation of the particles inside the trenches and the particles on the photoresist occurs because of the meniscus effect of the evaporating medium in the trenches,[22−25] and it lasts until either the concentration or the volume of the suspension stays in optimal ranges for the process. We have also attached additional images to show the relationship between the volume of suspension and the nature of the particle deposition and the clear separation of the particles inside the trenches from the ones on the resist. In order to verify theoretically that this phenomenon is general regardless of different parameters of the processes, we have performed the scaling analysis of the pressure and time scale of global and local fluid behaviors in the evaporating droplet in section 3. Also, the scaling effect of the patterning, the effect of the volume and the concentration of the suspension, and the effect of surface treatment are studied in section 3.

Release of Particle Assembly by Removal of Photoresist

Release of Microparticle Assemblies. After the particles are confined inside the trenches, the photoresist was dissolved by

(43) Adachi, E.; Dimitrov, A. S.; Nagayama, K. *Langmuir* **1995**, *11*, 1057.
(44) Schwartz, L. W.; Weidner, D. E. *J. Eng. Math.* **1995**, *29*, 91.

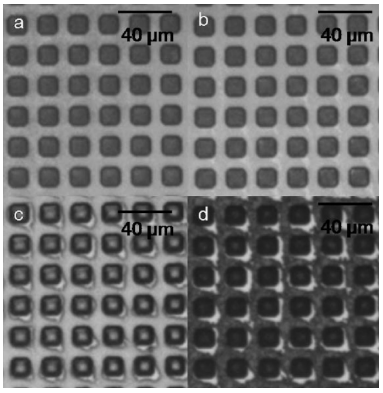

Figure 3. Magnified views of images from Figure 2 at the center of the droplet. (a) 3 s before the completion, the solutes are confined to the well (b) 2 s before the completion, slight evaporation of the medium is observed. (c) 1 s before the completion, the evaporation of the local fluid is initiated, and the separation of the fluid inside the well and outside the well is observed. (d) The evaporation is completed. The particle assemblies inside the trenches and outside the trenches are clearly separated.

remover (either acetone or PRS 3000 (J. T. Baker)) and microsphere-based 3D structures are released as shown in Figures 4 and 5. It is noteworthy that the packing structure can be preserved without any perturbation during the removal process of the photoresist. The assembled structure is preserved until the diameter of silica microspheres reaches 3 μm (the images of 3 μm silica microsphere-based structures are in Supporting Information); however, the structure is perturbed when the diameter is 5 μm. If the size of the particle decreases, the surface- to-volume ratio increases; thus, a stronger van der Waals force may preserve the particle assembly intact. Also, the surface charge condition of the particles is another crucial factor in the stability of the structures. The microstructure based on polystyrene microspheres (diameter $\sim$1 μm) is deteriorated after the photoresist removal. From these observations, one can conclude that the interparticle force of the assembled structure is dependent on the surface charge properties of the particles as well. Negatively charged colloidal particles, such as polystyrene, cannot withstand the photoresist removal process since the interparticle electrostatic repulsion force is stronger than the attractive force in nonpolar solvents.[45] It is anticipated that the smaller, insulating, or semiconducting particles will be more advantageous in line patterning than the larger and metallic particles. Uniform patterning of silica microsphere-based, high-aspect ratio structure is achieved inside the coffee-ring region as shown in Figure 4. An interesting feature is that the particles of the coffee-ring region where the excessive particles are connected to the particles inside the trenches form a bridge structure without collapse after the removal of the photoresist. This indicates that the attractive forces between the particles outdo the gravity force. This suspended structure can be potentially used for various MEMS (microelectromechanical systems) applications such as microfilters or cell sorting devices. Also, various structures are fabricated by adjusting the concentration of the suspension. By designing arbitrary geometries on photomask for photolithography with proper photoresist thickness set, a 3D pattern can be defined and this pattern can serve as an effective template to structure the particle assembly. The trenches comparable to the size of the single particles, lines, rectangle, and star-shapes are fabricated and used for the templates to pattern the particle assembly. In this patterning, the patterning area is designed to be smaller than the contact-line area of the droplet so that the bridge structure at the coffee-ring region is not formed. At the lift-off step, the particles located at the corner whose angle is smaller than 90° are harder to resolve because the excessive particles are driven by higher "over-pressure" gradient and attached to the particles inside the trenches. However, simple, symmetric patterns such as dots and lines are resolved well. If the spacing of the patterns is too small, or if the ratio of the particle diameter to the length of the pattern is too low, the patterns are not resolved well. It is found that the presented technique may not offer resolution as small as that of the previously reported technique;[22] however, it still holds the advantages in terms of 3D structuring of the assembly and superb simplicity. The commensurable effect was observed in the line and dot patterns. The number of the particles across the width ($=N_1$) is equal to [W(width)/D(particle diameter)] where function [x] returns the largest integer less than or equal to x. This effect is verified down to the limit of conventional contact-photolithography ($\sim$4 μm). The single particles (diameter, 3 μm), dots, and lines where the number of the particles (diameter, 1 μm) across the width is four are patterned. With the proper choice of dimensions of the template, desirable structures of the particle assembly can be fabricated as demonstrated. As stated previously, the corner effect causes an "over-pressure" gradient at the corner of the patterns hinged on the substrate. Therefore, the particles are transported to the corner first. In the case of lower-concentration suspension, fewer particles are transported to the corner until the evaporation of the droplet is completed; thus, ring-shaped structures are generated. As the concentration increases, the particles are deposited from the corner to the top of the pattern symmetrically as shown in Figure 5. By a simple multistep process, hybrid ring structures of the different-sized particles are fabricated too. This shows that the multilayer patterns can be easily formed by placing multiple different droplets in the same location in series.

Release of Nanoparticle Assemblies. The presented technique can be used for the patterning of semiconducting or metallic nanoparticle assembly. A droplet of monodispersed nanoparticle suspension is placed on the photopatterned substrate. If the nanoparticles are stabilized in the hydrophobic medium such as toluene, the oxygen-treated substrate is seated for 72 h to stabilize its surface charge and coated with HMDS (hexamethyldisilazane) to make its surface hydrophobic. Because oxygen plasma is used to make the surface hydrophilic and eliminate any probable residue of the photoresist, it is necessary even in the hydrophobic medium cases. As shown in Figure 6, TiO_2 nanoparticles (diameter, 70 nm) and ZnO nanoparticles (diameter, 30 nm) are assembled inside the various dimensions of trenches and patterns are generated after the removal of the photoresist. We intend to observe the "pure" interactions among the particles, medium, and patterns; thus, surfactant is not used for the stabilization of the nanoparticles in the suspension. Therefore, we believe the assembly to be the state of highly packed agglomerates, but not closely packed assembly. On the other hand, for the patterning of metallic nanoparticles, either surfactants need to be used or functional groups are required to be attached to the particles in order to disperse the nanoparticles in the suspension. A silver nanoparticle suspension (diameter, 7 nm) with amine dendrimer is synthesized according to the recipe in the literature[41] and patterned. 3D, high-aspect-ratio patterns are generated on the substrate. As shown in Figure 4, simple column structures, bridge structure, and ring structures are fabricated by simply controlling the concentration of the suspension. In particular, we expect the silver bridge structure to have potential significance in the

(45) Sainis, S. K.; Germain, V.; Mejean, C. O.; Dufresne, E. R. *Langmuir* **2008**, *24*, 1160.

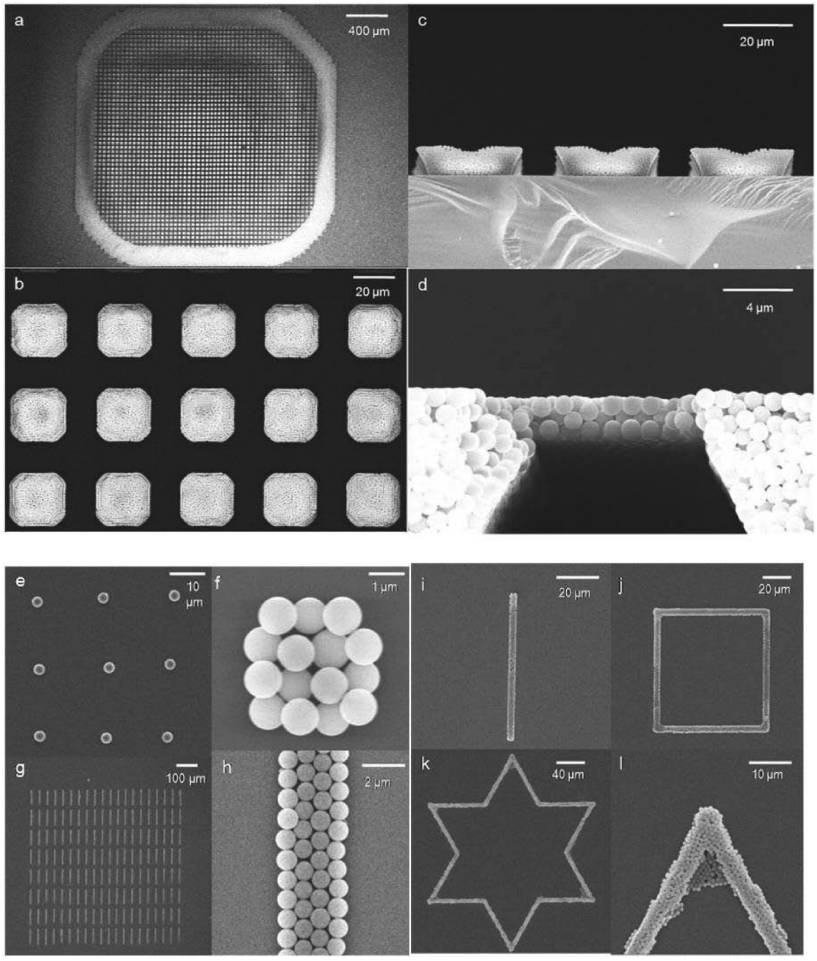

Figure 4. Images of the patterns of the microparticle assembly (after lift-off): (a) overall top view of the patterns, (b) close top view of the patterns, (c) cross-sectional view of the patterns, (d) bridge structure formed in the coffee-ring region. Various geometries of the patterns of microparticles: (e) patterns of single particles (diameter, 3 μm), (f) pattern of monolayer particle assembly (diameter, 1 μm), (g) line patterns of particle assembly (diameter, 1 μm), (h) close view of a single line, (i) overall view of single lines, (j) overall view of a rectangle, (k) overall view of a star, (l) close view of a star.

fabrication of metal interconnects, since it offers a simple, low-cost method to construct metal interconnects on IC (integrated circuits) chips.

Theoretical Analysis of Patterning

Scaling Analysis of Main Parameters in the Hydrodynamics of the Process. As mentioned in section 2.2, we have attempted the scaling analysis of the pressure and time scale of global and local fluid behaviors in the evaporating droplet in order to verify the validity of the process. Figure 7 shows an axisymmetric droplet on a horizontal substrate with the fluid density ρ^*, viscosity μ^*, initial height h_0^*, and initial radius r_0^*. The asterisk (*) denotes the dimensional parameters and the other denotes nondimensional parameters. The scales of global pressure P_1^* and global time t_1^* can be obtained from Fischer's model.[39]

The governing equations for the global fluid flow are

$$0 = \frac{1}{r}\frac{\partial}{\partial r}(ru) + \frac{\partial w}{\partial z} \tag{1}$$

$$0 = -\frac{\partial p}{\partial r} + \frac{\partial^2 u}{\partial z^2} \tag{2}$$

$$0 = -\frac{\partial p}{\partial z} \tag{3}$$

where radial velocity u^* is scaled by the characteristic viscous velocity, $u_c^* = \mu^*/\rho^* h_0^*$, pressure p^* is scaled by the characteristic pressure, $p_c^* = \mu^* u_c^* r_0^*/h_0^{*2}$, vertical velocity w^* is scaled by $\varepsilon u_c^* = \mu^*/\rho^* h_0^*$, and $\varepsilon = h_0^*/r_0^*$ is the ratio of the initial height to the initial radius of the droplet . Also, radius (r) and height (z) are nondimensionalized by the initial radius of the droplet, r_0^*, and the initial height of the droplet, h_0^*. The global, dimensionless radial velocity, u, to drive the particles from the center to the peripheral area can be expressed as

$$u = -\frac{1}{\mathrm{Ca}}\frac{\partial}{\partial r}\left[\frac{1}{r}\frac{\partial}{\partial r}\left(r\frac{\partial h}{\partial r}\right)\right]\left(\frac{1}{2}z^2 - hz\right) \tag{4}$$

where

$$\mathrm{Ca} = \frac{\mu^* u_c^*}{\varepsilon^3 \sigma^*} = \frac{\mu^{*2}}{\varepsilon^3 \rho^* \sigma^* h_0^*}$$

is the capillary number, μ^* is the viscosity of the medium, and σ^* is the surface tension of the liquid. The height (h^*) of the droplet is nondimensionalized by the initial height of the droplet, h_0^*.

Also, full height evolution profile can be expressed as[39]

$$\frac{\partial h}{\partial t} = -\frac{1}{3\mathrm{Ca}}\frac{1}{r}\frac{\partial}{\partial r}\left[rh^3\frac{\partial}{\partial r}\left(\frac{\partial^2 h}{\partial r^2} + \frac{1}{r}\frac{\partial h}{\partial r}\right)\right] - EJ \tag{5}$$

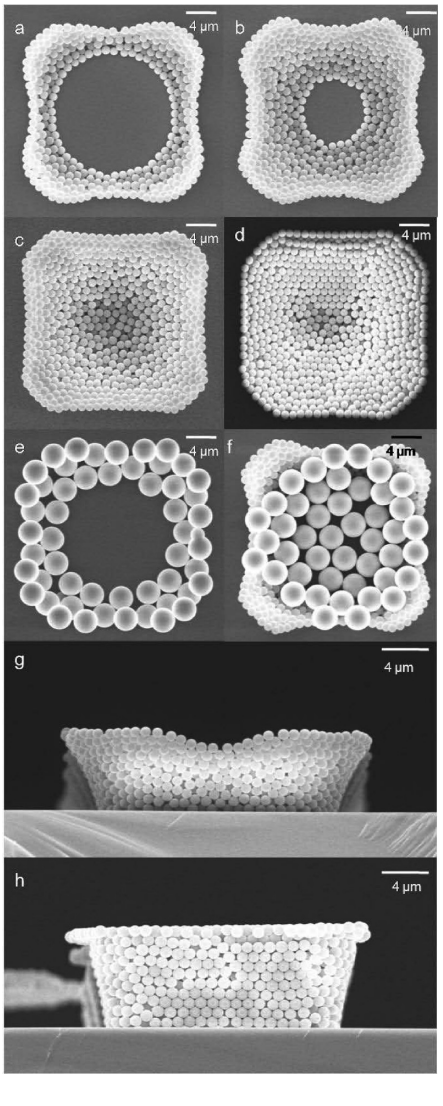

Figure 5. Dependence of the patterning with the concentration of the suspension. (a) 0.3125 wt % of the suspension (silica microspheres, diameter, 1 μm, 2 μL). (b) 0.625 wt % of the suspension (silica microspheres, diameter, 1 μm, 2 μL). (c) 1.25 wt % of the suspension (silica microspheres, diameter, 1 μm, 2 μL). (d) 2.5 wt % of the suspension (silica microspheres, diameter, 1 μm, 2 μL). (e) 0.3125 wt % of the suspension (silica microspheres, diameter, 3 μm, 2 μL). (f) A hybrid structure made by two 0.3125 wt % aliquots of the suspension of the different microspheres (silica microspheres, diameter, 3 μm (first), 5 μm (second), 2 μL). (g) A cross-sectional view of the pattern made from 2.5 wt % of the suspension (silica microspheres, diameter, 1 μm, 2 μL). (h) A cross-sectional view of the pattern made from 5 wt % of the suspension (silica microspheres, diameter, 1 μm, 2 μL).

where $E = k^*\Delta T^*/\varepsilon\mu^*L^*$ is the evaporation number and J is a spatially and time-dependent mass-flux, which is scaled by the characteristic mass flux $J_c^* = k^*\Delta T^*/h_0^*L^*$. On this scale, k^* is the thermal conductivity of the liquid, L^* is the heat of vaporization, and ΔT is the temperature difference between the temperature of the substrate and the saturation temperature. Time t was nondimensionalized by $t_c^* = r_0^*/u_c^*$. From the relations above, u can be scaled as 1/Ca; thus, the global pressure P_1^* can be scaled as $(1/\mathrm{Ca})(\mu^*u_c^*r_0^*/h_0^{*2})(p_c^*/\mathrm{Ca})$ from eq 2. Also, the global time t_1^* can be scaled as the larger one of either $\mathrm{Ca}t_c^*$ or t_c^*/E.

The scale of the local pressure P_2^* and the local time t_2^* can be obtained from Schwartz's model[39] of coating flows on curved surface, since the medium can be regarded as a thin coating layer on the curved substrate in the thin droplet. In Figure 6, (s, n) are local orthogonal coordinates with s being the arc-length along the surface and $n = h(s, t)$ the layer thickness to be determined. R^* is the mean curvature of the patterns. The expression for the pressure inside the coating flow is composed of two parts: "overpressure" distribution by the curvature of the patterned substrate (σ^*/R^*) and hydrodynamic effects by the fluid height ($\sigma^*(\partial^2h^*/\partial s^2)$).

$$p^* = -\frac{\sigma^*}{R^*} - \sigma^*\frac{\partial^2 h^*}{\partial s^2} \tag{6}$$

The height-evolution profile in dimensionless forms can be expressed as

$$\frac{\partial h}{\partial t} = -\frac{\partial}{\partial s}\left[h^3\left(\frac{\partial^3 h}{\partial s^3} + M\delta(s)\right)\right] \tag{7}$$

where $\delta(s)$ is the Dirac delta function. In our geometries, M can be expressed as $(\pi/4)(w^*/h_0^*)$ where w^* is the width of the pattern. Time t and height $h(s, n)$ was nondimensionalized by the larger of either $T^* = (3\mu^*w^{*4})/(\sigma^*h_0^{*3})$ or h_0^*. Therefore, the local pressure P_2^* can be scaled as either σ^*/R^* or σ^*h^*, and the local time t_2^* can be scaled as the larger of either T^* or T^*/M. In order for the particles to be confined in the trenches before the evaporation of the droplet is completed, two conditions are required: the local pressure has to be greater than the global pressure ($P_1^* \ll P_2^*$) around the patterns and the time for the particles to be transported from the droplet to the trenches has to be shorter than the time for the droplet to be evaporated. ($t_1^* \gg t_2^*$). If we input the experimental parameters of our processes (see the details of calculation in Supporting Information.), the scale of P_2^* is σ^*/R^*, the scale of t_1^* is t_c^*/E^* and the scale of t_2^* is T^*. Therefore, $P_2^*/P_1^* \approx r_0^{*2}/w^*h_0^* \gg 1$ and $t_2^*/t_1^* \approx (3k^*\Delta T^*u_c^*w^{*4})/(\sigma h_0^{*4}L^*) \ll 1$. This analysis indicates that the negative curvature of the radius of the patterns can serve as particle sinks while the convective transport of the medium drives the excessive particles to the edge of the droplet. It has an analogy with iron filings on paper where a series of magnets backing the paper withhold filings and wind blow eliminates extra filings where the magnetic force cannot reach. It is important to note that diffusion is not a major governing factor in the process. This can be easily verified by the comparison of the time scale of the diffusion process with the time scale of the convective transport, which has been already calculated previously. The time scale of diffusion, t_3, can be expressed as x^2/D where x is the travel distance of micro/nanoparticle and D is a diffusion coefficient of micro/nanoparticle in liquid. After we input the parameters of our process to the calcalculation (see the details of calculation in Supporting Information), it is $t_2^*/t_3^* \sim\ll 1$, which means that the process is completed much before diffusion plays a major role in the process; thus, diffusion can be neglected. The deposition of particles is mainly concentrated inside the trenches more than on the resist because of an overpressure gradient. If diffusion is dominant, the deposition of particles would be uniform throughout the entire droplet area; thus, the separation of the particles between the trenches and the resist cannot be achieved. Therefore, the separation of the particles can be attributed to the nature of the convective transport of the particles during the process.

Studies of Scaling Effect, Effect of Volume, and Concentration of Suspension on Patterning. After the particles are confined in the trenches, it is important for the particle assembly in the trenches to be separated from the particles on the photoresist,

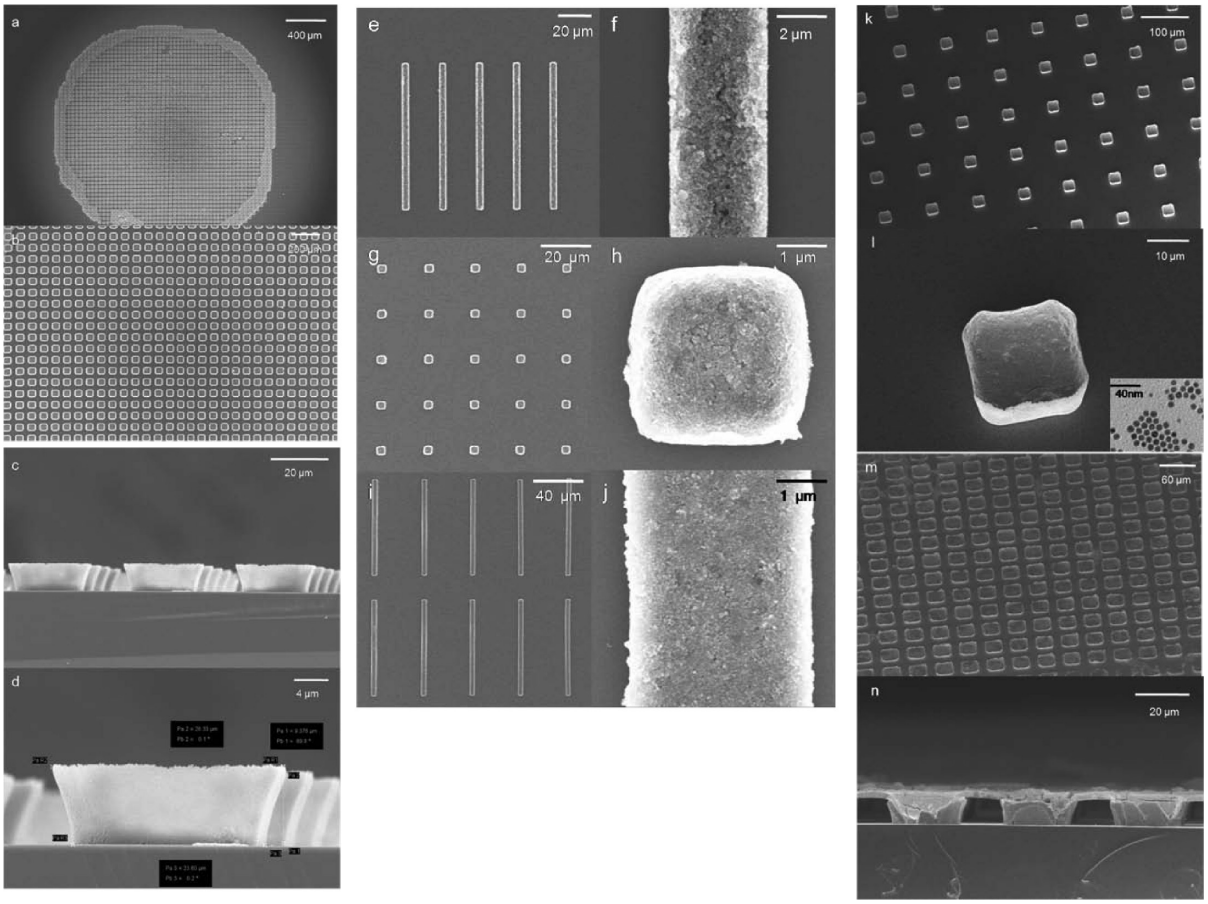

Figure 6. Images of the patterns of the nanoparticle assembly (after lift-off): (a) overall top view of TiO_2 patterns, (b) close top view of TiO_2 patterns, (c) cross-sectional view of TiO_2 patterns, (d) cross-sectional view of a single TiO_2 pattern. Various geometries of the patterns of semiconducting nanoparticles: (e) overall view of TiO_2 line patterns, (f) close view of a single TiO_2 line pattern, (g) overall view of ZnO dot patterns, (h) close view of a single TiO_2 dot pattern, (i) overall view of ZnO line patterns, (j) close view of a single ZnO line pattern. Various geometries of the patterns of metallic nanoparticles: (k) overall view of Ag dot patterns, (l) close view of a single Ag dot pattern. The image at the bottom right-hand corner is a TEM images of Ag nanoparticles (average diameter: 7 nm) used in the experiment, (m) overall view of Ag ring-shaped patterns, (n) cross-sectional view of Ag bridge patterns.

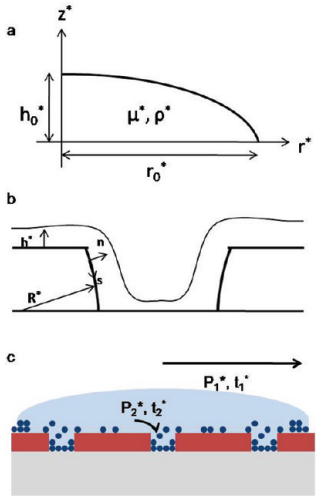

Figure 7. Notations for the scaling analysis. (a) Global coordinates with respect to the droplet. (b) Local coordinates with respect to a single pattern. (c) Schematic of the definition of global, local pressure and time.

since the particle assembly inside the trenches should not be perturbed by the particles on the photoresist during lift-off processes. Therefore, it is important to adjust process parameters such as the length scale of the trenches, the volume, the concentration of the suspension, and the surface charge condition in order to fill the trenches completely without being connected to the particles on the photoresist. At first, the scaling effect of the patterning is studied by the experiments of four different length scales. The details of the experiments are described in Experimental section. The volume of the suspension used for the patterning is determined in such a way that the number of particles per unit area of the patterning is constant throughout the experiments of different length scales. The analysis shows that there is an optimal range of the length scale of trenches and the particles for effective patterning by using presented technique. As shown in Figure 8, the packing volume ratio (defined as (the volume of occupied particles)/(the volume of particles at complete filling of the trenches); the details of the calculations are described in Supporting Information) increases at a given weight fraction of the particles as the length scale increases. This implies that a smaller weight fraction of the particles is required to achieve the complete filling of the trenches in the case of larger length scales. The previous scaling analysis shows that $P_2^*/P_1^* \approx r_0^{*2}/w^*h_0^*$ remains constant regardless of the length scales; however, $t_2^*/t_1^* \approx (3k^*\Delta T^*u_c^*w^{*4})/(\sigma h_0^{*4}L^*)$ is proportional to $\Delta T^*u_c^* \propto \Delta T^*/h_0^*$. Assuming the change of ΔT^* is negligible in different length-scales, t_2^*/t_1^* decreases as the length-scale increases. Therefore, the required time for the global transportation of the

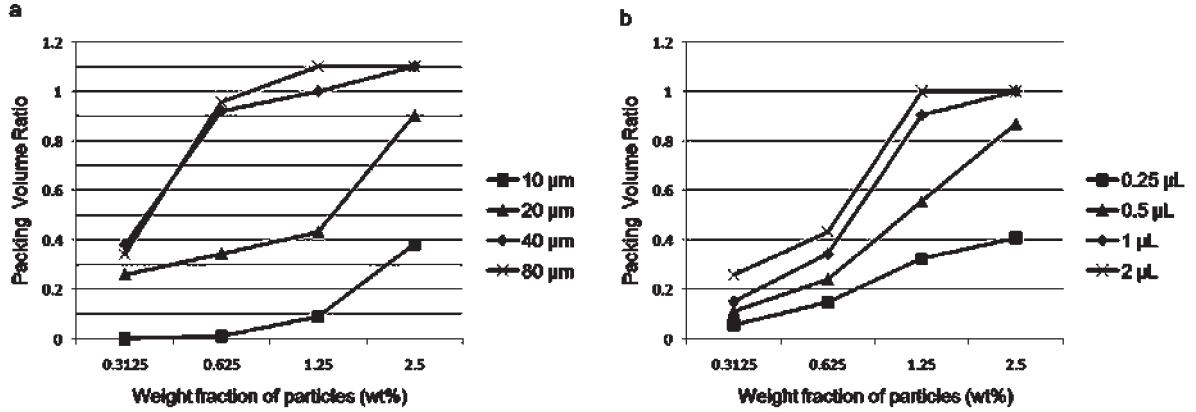

Figure 8. Graphs of the packing volume ratio versus the weight fraction of a suspension. (a) Graph of scaling effect. The packing volume ratio, 1, refers to the complete filling of the trenches without interconnection between particles inside the trenches and outside the trenches. The packing volume ratio over 1 indicates that the particle assembly inside the trenches to the particles on the photoresist are connected. (b) Graph of volume effect.

particles from the center of the droplet to the edge of the droplet becomes relatively larger in the larger length-scale, and more particles are inclined to be confined to the trenches than transported to the edge of the droplet. This analysis indicates that the patterning of smaller particles in smaller length-scale trenches requires a highly concentrated suspension which is harder to make in nanoparticle synthesis. Furthermore, the size of the droplet required for uniform patterning is inversely proportional to (length scale of the pattern)^3 and the size of the droplet has to shrink down significantly in smaller-scale patterning; however, generating ultrasmall droplets is also a challenge. Although the patterning of larger particles in larger length-scale patterns requires a smaller weight fraction of the suspension, the patterning in large scale requires long process time because the time for the droplet to evaporate correlates approximately with the length scale^2 (see Supporting Information for verification of this claim.). Also, extremely low concentration of the suspension which is needed in very large-scale patterning also undermines effective patterning because the deposition of the particle assembly is nonuniform and stripe patterns of the particle assembly are formed over the entire area of the droplet.[42] Therefore, the right dimensions of the trenches and the particles have to be chosen, considering the trade-off between the concentration of the suspension and process time. The dependence of the packing volume ratio on different volume of the suspension is studied at the fixed length scale of the trenches. The higher concentration and the larger volume of the suspension increase the packing volume ratio. As can be seen from Figure 8, there exist optimal ranges of the volume, the concentration of the suspension for complete filling of the particles in the trenches without overflow in the given length scale of the trenches.

Besides volume and concentration of the suspension, other factors such as humidity or temperature might affect the optimal range of volume and concentration of the suspension. For instance, if the humidity increases, the evaporation rate of the droplet will decrease and the evaporation time will be longer. Then, more particles are likely to be transported to the edge of the droplet and fewer particles stay and deposit onto the trenches. Therefore, higher concentration of the suspension will be required for optimal packing of the particles in the trenches. Systematic experiments by controlling humidity and temperature of the experimental environment need to be carried out to study the effect of those factors.

Studies of Surface Charge Condition of Templates on Patterning. Surface charge condition is another crucial parameter to achieve uniform, well-defined patterning of particle

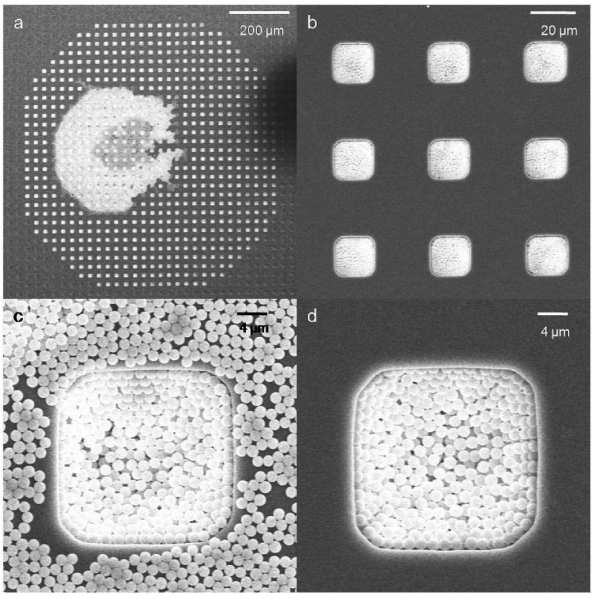

Figure 9. Images of the confinement of the particle assembly on a photopatterned substrate without surface treatment (before lift-off). (a) Overall view of the patterns. (b) Patterns in the peripheral area of the droplet. (c) Pattern in the central area of the droplet. (d) Pattern in the peripheral area of the droplet.

assembly. If the surface of the photopatterned substrate is not treated by oxygen plasma, the contact angle of the droplet of the suspension with respect to the substrate increases and Marangoni flow causes the nonuniform deposition of the particles. Marangoni flow is generated by the thermal gradient induced by the different evaporative rate inside the droplet and the direction of this flow is from the edge of the droplet to the center.[40,41] Marangoni number, the indicator of Marangoni flow, is the ratio of the Marangoni force to viscous force and represented as $\mathrm{Ma} \equiv -\beta \Delta T_0 t_f / \mu R$ where $\beta = \mathrm{d}\sigma/\mathrm{d}T$, ΔT_0 is the temperature difference between the edge and the top of the droplet, t_f is drying time, R is the radius of contact line radius. If the contact angle increases, R decreases at the fixed volume of the suspension and t_f increases because the surface-to-volume decreases. Also, ΔT_0 increases because the vertical distance between the top of the droplet and the edge of the droplet increases, and a higher temperature gradient is required to transfer the same amount of the heat. Therefore, Ma increases and Marangoni flow reverses the coffee-ring effect. As shown in Figure 9, when the patterning

was achieved without the treatment of oxygen plasma, the Marangoni effect caused the particles to be transported from the edge of the droplet to the center and more particles are deposited in the center than the edge of the droplet. It is noteworthy that the complete packing of the particles without any particle on the photoresist is observed in the peripheral area of the droplet. Without the treatment of oxygen plasma, the photoresist remains hydrophobic while the substrate is still hydrophilic. The particles in water medium are driven by the corner effect of the trenches as well as the surface-tension gradient created by the different surface energies between the photoresist and the substrates. The excessive particles after complete packing of the particles in the trenches are mainly driven by Marangoni flow without being left on the surface of the photoresist because the hydrophobic surface of the photoresist drives the particles to the Marangoni flow. This interesting physical phenomenon may not be suitable in large area patterning of particle assembly because of the nonuniformity caused by Maragoni effect; however, it can be used effectively for local patterning of micro/nanoparticle assembly in the micro/nanoscale with the low concentration suspension in the followed lift-off process.

In addition, the surface charge of the substrate is believed to enhance the adhesion force between the particle assemblies and the substrate since hydrophilic functional group of the substrate and the particle will generate attractive force and will hold them together.

Conclusions

We have demonstrated very simple, effective methods to pattern 3D micro/nanoparticle assembly by taking advantage of evaporative self-assembly and the coffee-ring effect of an evaporating droplet of a low-concentration suspension. Because of its great simplicity, wide applicability to various materials, and compatibility with existing photolithographic processes, we anticipate that this simple technique will be widely used in the fabrication of 3D photonic crystals and as key components in low-cost electronics/MEMS and will also provide an accurately tunable platform to study interesting electrical and optical properties of the particle assembly with microsize apparatus on-chip.

Acknowledgment. This research is supported by a grant (2009K000069) from Center for Nanoscale Mechatronics & Manufacturing (CNMM), one of the 21st Century Frontier Research Programs, which are supported by Ministry of Education, Science and Technology, Korea and U.S. Department of Energy (DOE, Grant #: DE-AC02-05CH112). S. Choi also thanks for his graduate fellowship from Samsung Scholarship Foundation.

Supporting Information Available: Relationship between volume of suspension and nature of particle deposition and the calculation of the scaling analysis is attached. Also, the details of the calculation of packing volume ratio are included. This material is available free of charge via the Internet at http://pubs.acs.org.